Weyl fermions with various chiralities in an *f*-electron ferromagnetic system: PrB_4

Dong-Choon Ryu,[1,2,3,*] Junwon Kim,[1] Kyoo Kim,[4] Bongjae Kim,[2,5] Chang-Jong Kang,[3,6,†] and B. I. Min[1,‡]

[1]*Department of Physics, Pohang University of Science and Technology, Pohang 37673, Korea*
[2]*Department of Physics, Kunsan National University, Gunsan 54150, Korea*
[3]*Department of Physics, Chungnam National University, Daejeon 34134, Korea*
[4]*Korea Atomic Energy Research Institute, Daejeon 34057, Korea*
[5]*Department of Physics, Kyungpook National University, Daegu 41566, Korea*
[6]*Institute of Quantum Systems, Chungnam National University, Daejeon 34134, Korea*

(Received 19 December 2023; revised 23 July 2024; accepted 14 August 2024; published 27 August 2024)

Rare-earth tetraborides (RB_4) have attracted a lot of recent attention due to their intriguing electronic, magnetic, and topological properties. We have theoretically investigated the topological properties of PrB_4, which is unique among the RB_4 family due to its ferromagnetic ground state. We have discovered that PrB_4 is an intrinsic magnetic Weyl system possessing multiple topological band crossings with various chiral charges. Density-functional-theory band calculations combined with a tight-binding band analysis reveal large Fermi-arc surface states, which are characteristic fingerprints of Weyl fermions. Anomalous Hall conductivity is estimated to be very large, ranging from 500 to 1000 $(\Omega\,\mathrm{cm})^{-1}$ near the Fermi level, which also demonstrates the topological Weyl character of ferromagnetic PrB_4. These findings suggest that PrB_4, being a potential candidate of a magnetic Weyl system, would be a promising rare-earth topological system for applications to next-generation spintronic and photonic devices.

DOI: 10.1103/PhysRevB.110.075156

I. INTRODUCTION

The Weyl semimetal is a topological system, which has attracted a lot of recent attention in the condensed matter physics community [1–3]. A Weyl semimetal is featured by exotic bulk Weyl points of twofold-degenerate band crossings and associated topological Fermi-arc surface states. Due to the inherent chiral-anomaly nature of Weyl fermions, the Weyl system exhibits negative longitudinal magnetoresistance. In addition, unusual phenomena of the chiral magnetic effect, the giant anomalous Hall effect, and the large magneto-optical Kerr effect are supposed to be realized in Weyl systems as a consequence of the chiral anomaly [2–4]. The emergence of Weyl fermion excitation requires the breaking of either time-reversal (T) or spatial inversion (P) symmetry, because the existence of both symmetries produces Kramers degenerate bands for all $\mathbf{k}$, and thereby any band crossing has fourfold degeneracy.

Since the pioneering study of a Weyl semimetal on T-breaking pyrochlore iridates [1], subsequent studies of Weyl systems have focused on P-breaking materials, and so most of the reported Weyl systems belong to noncentrosymmetric crystals, such as transition-metal monophosphides and dichalcogenides [5–8]. In contrast, T-breaking magnetic Weyl systems (MWSs) are relatively less explored. Following earlier theoretical reports on the MWS candidates of $Y_2Ir_2O_7$ [1], $HgCr_2Se_4$ [9], and $SrRuO_3$ [10], only a few more materials such as GdBiPt [11,12], CeSb [13], and GdB_4 [14] have been proposed as MWS candidates. These systems, however, demand manipulation of the external magnetic B field to generate Weyl points or to stabilize the magnetic ordering, and so experimental investigations were limited. Moreover, for CeSb, an angle-resolved photoemission (ARPES) study raised a question about the existence of band inversion and the emergence of Weyl fermions [15].

More recently, the Heusler-based Co_2MnGa [16,17], and kagome-lattice-based Mn_3Sn [18] and $Co_3Sn_2S_2$ [19,20] were reported to be MWSs. In the cases of rare-earth systems, PrAlGe, in which both P and T are broken, was proposed to be an MWS candidate [21,22]. Also, EuB_6 was reported to be a candidate for a T-breaking MWS [23,24]. Hence, there are only a number of genuine T-breaking MWS candidates, and they are mostly d-electron systems.

In this paper, we have investigated topological properties of a representative rare-earth tetraboride system, PrB_4, and found that PrB_4 is a genuine T-breaking MWS with f electrons. With its intrinsic ferromagnetism, PrB_4 possesses a unique Weyl fermion character with various types of chiral charges. Note that rare-earth tetraborides RB_4 (R: rare-earth elements) exhibit diverse magnetic ground states, depending on the R element, such as Kondo, ferromagnetic (FM), and antiferromagnetic (AFM) states. Furthermore, exotic topological properties were also predicted for tetraborides. As mentioned above, GdB_4, having an in-plane noncollinear AFM ground state of a well-known Shastry-Sutherland lattice type, was proposed to be a Weyl system in the presence of the external B field [14]. Albeit not RB_4, an actinide-tetraboride

*Contact author: dcrhyu@postech.ac.kr
†Contact author: cjkang87@cnu.ac.kr
‡Contact author: bimin@postech.ac.kr

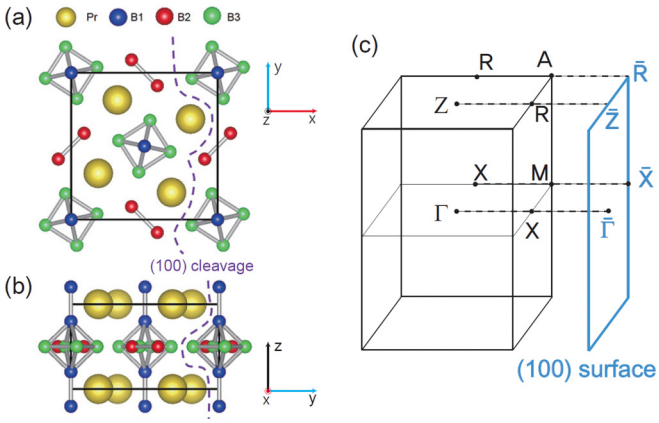

FIG. 1. Tetragonal crystal structure of PrB_4 with nonsymmorphic $P4/mbm$ space group. (a) Top view and (b) side view. Purple dashed lines indicate (100) surface cleavage we have considered for the Pr termination in Fig. 3. (c) Bulk and (100) surface BZ.

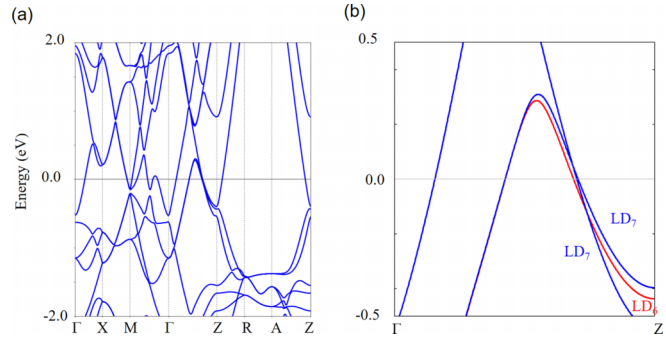

FIG. 2. (a) Bulk band structure of nonmagnetic PrB_4 obtained by the $4f$ open-core calculation, including the spin-orbit coupling. (b) Amplified band structure near E_F along Γ-Z with the corresponding irrep for each band. The band with the irrep of LD_6 is drawn in red for clarity.

Kondo system, PuB_4, was reported to host intriguing fourfold-degenerate topological wallpaper fermions on its surface [25]. Similarly, DyB_4, which has a noncollinear AFM ground state, was reported to host magnetic wallpaper fermions [26].

PrB_4 is unique in that it is a sole ferromagnet among RB_4. According to a magnetic susceptibility experiment [27], upon cooling, PrB_4 shows first the AFM ordering at $T_N \sim 19.5$ K, and then the FM ordering below $T_C \sim 15.9$ K. In view of the B-field-induced MWS for AFM GdB_4, PrB_4 in the FM phase is expected to have a Weyl-type band structure even in the absence of an external B field. Indeed, for PrB_4, we have theoretically found that Weyl fermions with various chiral charges emerge in its FM ground state with associated topological Fermi-arc surface states. Also, the estimated anomalous Hall conductivity (AHC), which originates from the large Berry curvature contributed by some Weyl nodes and band anticrossings, reaches as high as 1000 $(\Omega\,\mathrm{cm})^{-1}$, which corroborates that PrB_4 is a candidate of intrinsic rare-earth MWS.

II. CRYSTAL STRUCTURE AND COMPUTATIONAL DETAILS

PrB_4 crystallizes in a tetragonal structure with the nonsymmorphic $P4/mbm$ space group (SG 127). In Fig. 1, the crystal structure of PrB_4 and its bulk and surface Brillouin zone (BZ) are depicted. The lattice constants and internal coordinates used in this study were adopted from the experiment ($a = 7.235$ Å, $c = 4.116$ Å) [28].

For the first-principles density-functional-theory (DFT) band calculations, we have employed the projector augmented-wave (PAW) band method implemented in VASP in the generalized gradient approximation (GGA) [29–31]. To describe the strongly correlated Pr $4f$ electrons, we have used the GGA+U calculations with Coulomb (U) and exchange (J) correlation parameters. We set the parameters for $U = 4$ eV, which is a commonly accepted value for the Pr atom [32,33], and $J = 0.4$ eV, which reproduces well the observed magnetic moment of $2.1\mu_B$ per Pr atom [27] (see Fig. S1 in the Supplemental Material [34]).

Surface electronic structures and chiral charges of Weyl points are obtained based on a Wannierized tight-binding Hamiltonian [35] by utilizing the WANNIERTOOLS code [36]. We have also obtained the Berry curvature and estimated the anomalous Hall conductivity based on the Wannierized tight-binding bulk band structures.

III. BULK BAND STRUCTURE OF NONMAGNETIC PrB_4

Figure 2(a) shows the bulk band structure of PrB_4 obtained by the so-called "open-core" calculations, in which Pr $4f$ electrons are treated as the core, so that the magnetism is suppressed. In Fig. 2(b), the amplified band structure near the Fermi level (E_F) along Γ-Z is plotted with the irreducible representation (irrep) of each band. Every band along Γ-Z is twofold degenerate due to the time-reversal pairing, and so the fourfold-degenerate band crossing can occur when two bands of distinct irreps of LD_6 and LD_7 intersect, as shown in Fig. 2(b). Since the system preserves both the inversion P and time-reversal T symmetries in the absence of magnetism, any fourfold band crossing in this system must manifest itself as a Dirac point. Note that the Dirac point shown in Fig. 2(b) is of type-II nature. Surface states relevant to those Dirac points are further discussed in the Supplemental Material (Fig. S3) [34].

IV. WEYL POINTS AND FERMI ARCS

Now we discuss the role of the magnetism in the emergence of the Weyl fermions in PrB_4. First, we have investigated the energetics of three different magnetic structures of PrB_4, FM and two types of AFM, and found that the FM state is indeed a ground state with magnetic ordering along the (001) direction, which is in agreement with the experimental results (see Fig. S2 and Table S1 in the Supplemental Material [34]). Then the formation of Weyl points, when breaking the time-reversal symmetry, is examined on the basis of the model Hamiltonian obtained from the nonmagnetic calculation by taking into account a Zeeman-like term (see Figs. S5 and S6 in the Supplemental Material [34]).

In order to examine the existence of Weyl points and their associated Fermi-arc surface states, we have investigated the

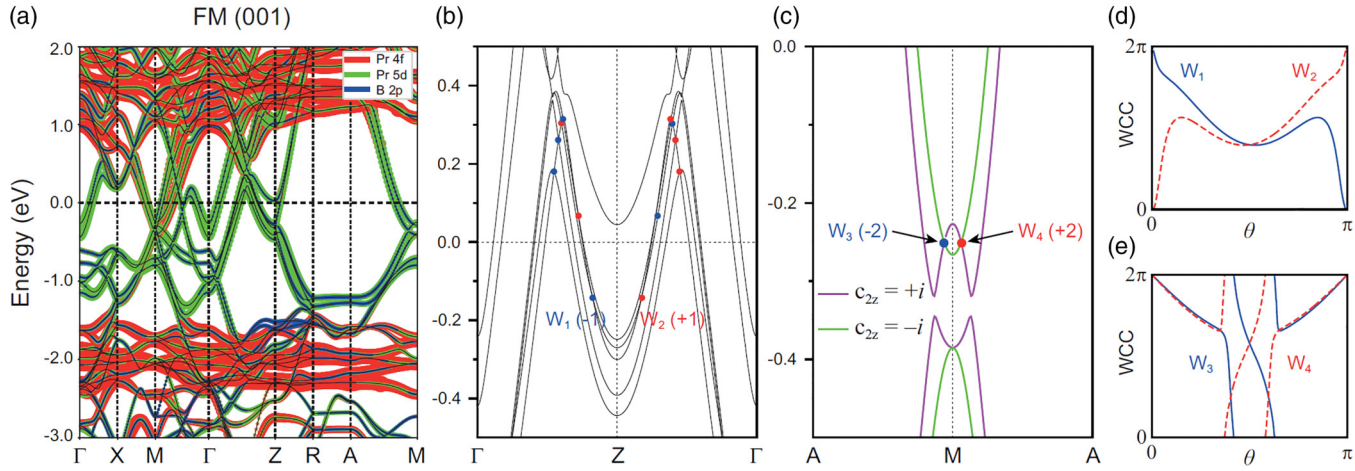

FIG. 3. (a) Bulk band structures of PrB_4 with FM ordering along the (001) direction. (b), (c) Bulk band structures along rotationally invariant paths Γ-Z-Γ and A-M-A under the FM ordering. The Weyl points of topological band crossings are represented by red and blue dots, depending on their chiral charges. (d), (e) Evolution of Wannier charge center (WCC) on the spheres centered at four Weyl points W_1–W_4 marked in (b) and (c).

band structures of FM PrB_4 with (001) magnetic ordering. Figure 3(a) shows that Pr $4f$ states are located near -2 and 2 eV, while wider Pr $5d$ and B p bands are located near the Fermi level E_F.

The high-symmetry k paths, namely Γ-Z and M-A, are invariant under C_{4z} and C_{2z} rotations, as shown in Fig. 1, which leads to the occurrence of band crossings along those two paths. Indeed, the band crossings in the vicinity of E_F are clearly manifested in Figs. 3(b) and 3(c) along Γ-Z-Γ and A-M-A paths, respectively. The red and blue dots represent the Weyl points with positive and negative chiralities, respectively, which are identified from the Wilson loop calculations. There are several Weyl points along Γ-Z, while there is only one along A-M near E_F (see Table S2 in the Supplemental Material [34]).

Notable in Figs. 3(b) and 3(c) is that Weyl points on the Γ-Z path are conventional twofold-degenerate Weyl nodes, but those on the M-A path, W_3 and W_4, are exotic fourfold-degenerate Weyl nodes, arising from the unique crystal symmetry of FM PrB_4. Because of the magnetic ordering, the T symmetry is not preserved here, but the combination of T and a nonsymmorphic screw-axis symmetry, $S_y = \{C_{2y}|\frac{1}{2}\frac{1}{2}0\}$, is preserved. Interestingly, this combined symmetry S_yT makes every band on the M-A path doubly degenerate even under the FM ordering. To be more specific, for any eigenstate ψ on M-A, there exists its Kramers pair $S_yT\psi$ since $(S_yT)^2 = \exp(ik_x) = -1$ on M-A [note that both M and A have $(k_x, k_y) = (\pi, \pi)$]. Furthermore, when $C_{2z}\psi = \pm i\psi$, we have $C_{2z}(S_yT\psi) = -\exp[i(k_x + k_y)]S_yTC_{2z}\psi = \pm i(S_yT\psi)$. Namely, two bands in each Kramers pair have the same C_{2z} eigenvalues, which suggests that some accidental band crossings between two Kramers pairs with distinct C_{2z} eigenvalues can be preserved by crystal symmetry. In fact, the Wannier charge center (WCC) calculations in Figs. 3(d) and 3(e) confirmed that the chiralities (topological charges: χ's) of (W_1 and W_2) and (W_3 and W_4) Weyl points are $\chi = \pm 1$ and $\chi = \pm 2$, implying single-Weyl and double-Weyl points, respectively. The existence of both single- and double-Weyl points in PrB_4, albeit somewhat complicated, would be more effective for applications to topological devices, as in the case of chiral fermion systems with multifold degeneracy [37,38].

To confirm the Fermi arcs, which are one of the hallmarks of Weyl fermions, the surface electronic structure calculations were carried out. Although the (001) surface is the natural cleavage plane of PrB_4, the (100) surface is more preferable to identify the Fermi arcs more clearly. On the (001) surface, all the Weyl points on Γ-Z and M-A are to be projected onto $\bar{\Gamma}$ and $\bar{M}$, respectively. This results in the overlap of Weyl points of opposite chiralities and, as a consequence, no vestige of the Fermi arcs. So we have examined the surface electronic structures on the (100) surface.

Figure 4 shows the two different sets of possible Fermi arcs depending on the surface terminations. In Fig. 4(a), which displays constant-energy surfaces for the Pr termination, a few surface states presumed to be Fermi arcs are observed near $\bar{Z}$, and those Fermi arcs become larger for a higher-energy cut. In Fig. 4(c) surface band structures are plotted along $\bar{\Gamma}$-$\bar{Z}$-$\bar{\Gamma}$ and $\bar{R}$-$\bar{Z}$-$\bar{R}$, in which three surface states SS_1–SS_3 are identified. A comparative analysis of Figs. 4(a) and 4(c) suggests that SS_1 corresponds to the largest Fermi arc shown in Fig. 4(a) connecting two charge-opposite Weyl points at a higher energy, slightly below $E = 0.3$ eV, while SS_2 and SS_3 connect four Weyl points close to $\bar{Z}$. On the other hand, for the B termination of Fig. 4(b), putative Fermi arcs are buried in the bulk Fermi surface near $\bar{Z}$ and so are difficult to be discerned. Nevertheless, Figs. 4(b) and 4(d) reveal that there is a narrow band gap at $\bar{Z}$ near $E = -0.25$ eV, and Fermi arcs can be resolved in the gap region.

In contrast, the Fermi arcs arising from the double-Weyl points are difficult to identify, because they are mostly buried within the bulk continuum. Nevertheless, surface band-structure and constant-energy surface calculations in Fig. 5 show that one of the long tails connected to those double-Weyl points [indicated by white arrows in Figs. 5(c) and 5(d)] is partially revealed between $\bar{X}$-$\bar{R}$. Indeed, the zoomed-in figures in Figs. 5(c) and 5(d) (the rightmost figures) clearly show the

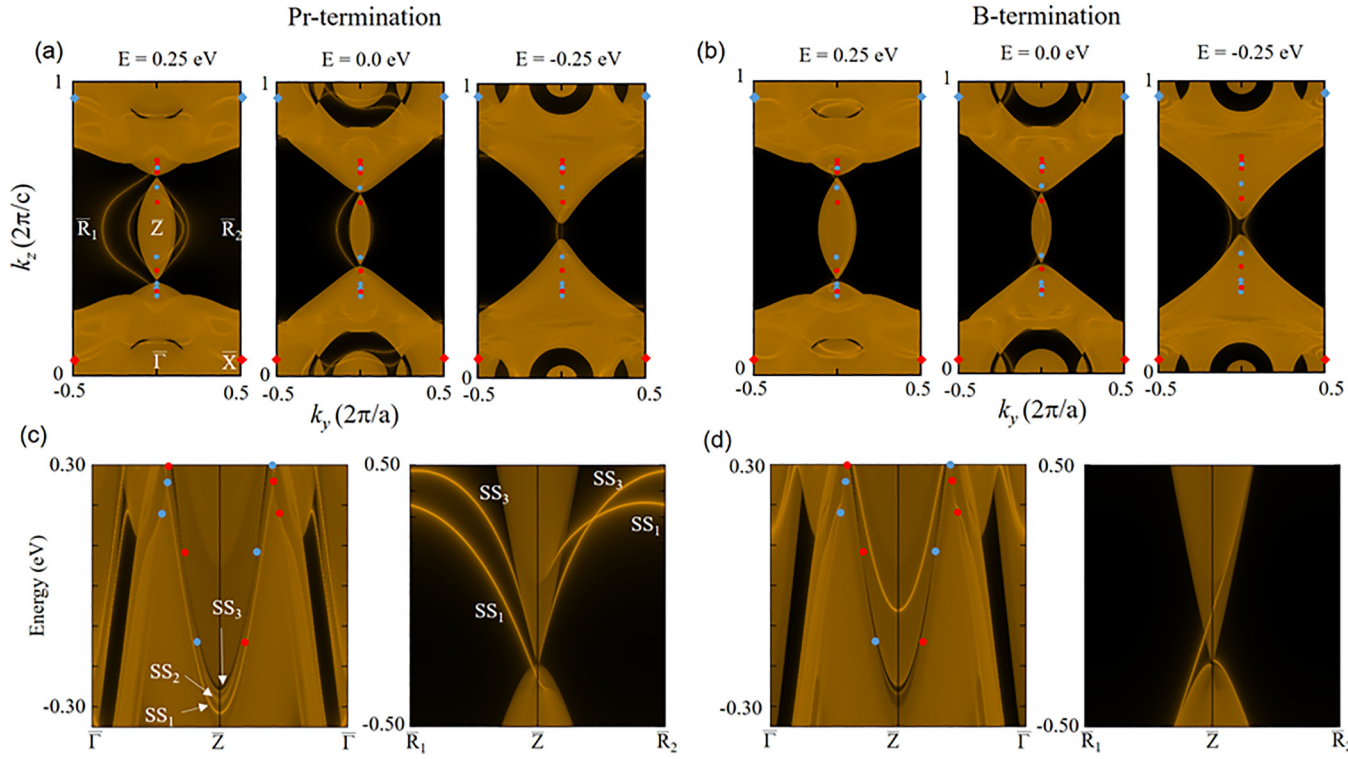

FIG. 4. Surface electronic structures on (100) surface of FM PrB_4. (a), (b) Constant-energy surfaces at various energy levels with Pr and B termination, respectively. Red and blue circles (diamonds) indicate the positions of Weyl fermions with chiralities $\chi = \pm 1$ ($\chi = \pm 2$), respectively. (c), (d) Surface band structures along $\bar{\Gamma}$-$\bar{Z}$-$\bar{\Gamma}$ and $\bar{R}_1$-$\bar{Z}$-$\bar{R}_2$. Red and blue dots denote the positions of Weyl points with positive and negative chiral charges, respectively.

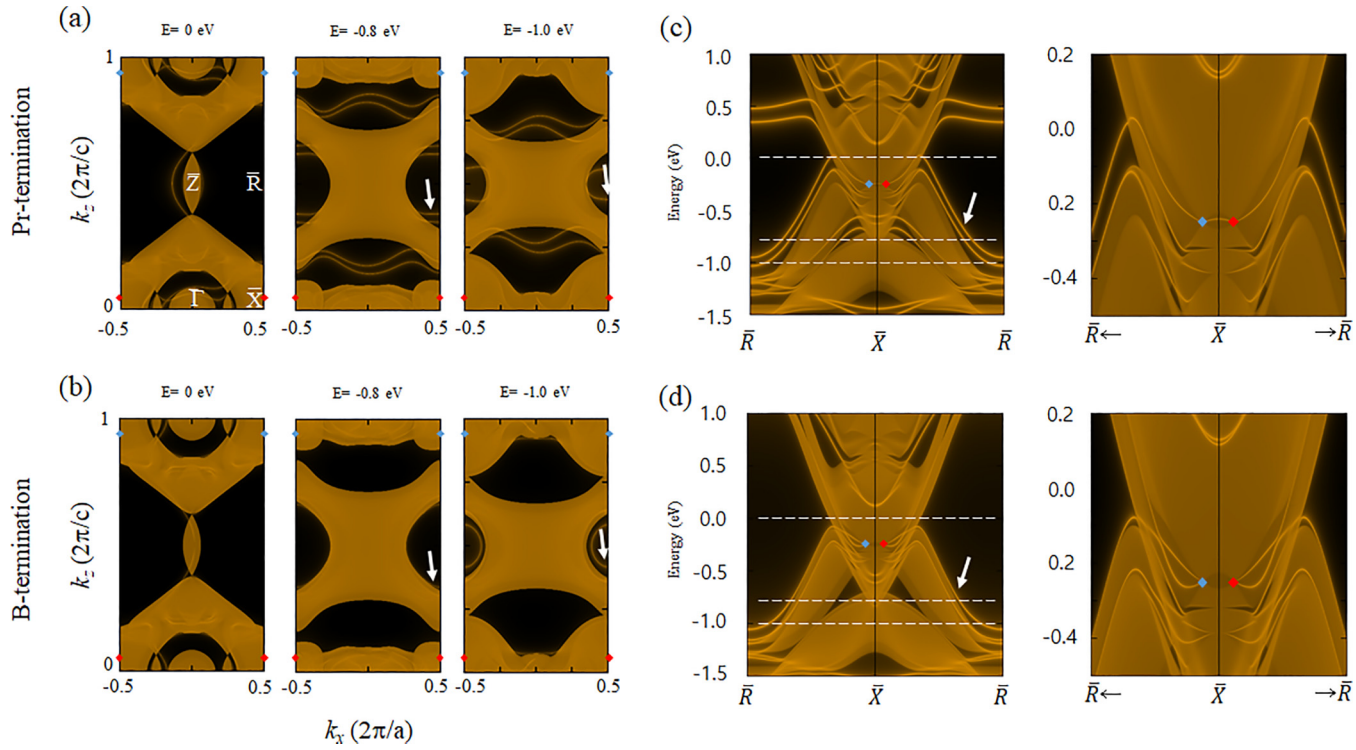

FIG. 5. (a), (b) Constant-energy surfaces at various energy levels, and (c), (d) surface band structures of the ferromagnetic phase of Weyl semimetallic PrB_4 for (top) Pr and (bottom) B termination. The rightmost figures correspond to the amplified plots of the left figures in (c) and (d). The positions of double-Weyl fermions with chirality $|\chi| = 2$ are denoted by red (positive) and blue (negative) diamonds in the figure. Surface Fermi-arc states connected to the double-Weyl fermions are indicated by white arrows. The dashed lines in (c) and (d) represent the energy levels of the constant-energy surfaces in (a) and (b).

emergence of associated surface states from the double-Weyl points, despite being buried within the bulk continuum.

It is worthwhile to compare the topological properties of PrB_4 depending on its different magnetic states. As discussed earlier, we have shown that nonmagnetic PrB_4 is a Dirac semimetal, hosting a type-II Dirac point along Γ-Z. For AFM PrB_4, we have found that it can be either a trivial normal metal (AFM1 configuration) or MWS (AFM2 configuration) depending on magnetic configurations, as demonstrated in Figs. S2 and S4 of the Supplemental Material [34]. However, the AFM2 MWS state does not host a Weyl point on Γ-Z nor does a double-Weyl point on M-A. Instead, it hosts Weyl points on the generic k points near M (see Table S3 in the Supplemental Material [34]). Notably, PrB_4 exhibits a unique temperature-dependent variation in magnetic ordering upon cooling, transitioning from paramagnetic (PM) to AFM and finally to FM states. This leads to a topological phase transition from a topological Dirac semimetal to an intermediate AFM metal and, ultimately, to a magnetic Weyl semimetal as the temperature decreases. This property allows for the utilization of temperature-tuned topological properties in PrB_4.

V. ANOMALOUS HALL CONDUCTIVITY (AHC)

In MWSs, the AHC, which is much larger than the ordinary Hall conductivity, originates from intrinsic topological properties of the band structure, specifically the Berry curvature. We have estimated the AHC, $\sigma_{\alpha\beta}$, using the following equations [39],

$$\sigma_{\alpha\beta} = -\frac{e^2}{\hbar}\int_{\mathrm{BZ}} \frac{d\boldsymbol{k}}{(2\pi)^3}\Omega_{\alpha\beta}(\boldsymbol{k}), \tag{1}$$

where $\Omega_{\alpha\beta}(\boldsymbol{k})$ is the total Berry curvature,

$$\Omega_{\alpha\beta}(\boldsymbol{k}) = -2\,\mathrm{Im}\sum_{v}\sum_{c}\frac{v_{vc,\alpha}(\boldsymbol{k})v_{cv,\beta}(\boldsymbol{k})}{[\epsilon_c(\boldsymbol{k})-\epsilon_v(\boldsymbol{k})]^2}. \tag{2}$$

Here, $\epsilon_n(\boldsymbol{k})$ is the energy of the nth band at $\boldsymbol{k}$, c and v denote unoccupied and occupied bands, and the velocity $v_{nm,\alpha}(\boldsymbol{k})$ is given by

$$v_{nm,\alpha}(\boldsymbol{k}) = \langle\psi_{n\boldsymbol{k}}|\hat{v}_\alpha|\psi_{m\boldsymbol{k}}\rangle = \frac{1}{\hbar}\langle u_{n\boldsymbol{k}}|\frac{\partial\hat{H}(\boldsymbol{k})}{\partial k_\alpha}|u_{m\boldsymbol{k}}\rangle. \tag{3}$$

For the FM state with magnetic ordering along the (001) direction, the mirror symmetry M_z is present, which prohibits the σ_{yz} or σ_{zx} component, resulting in only σ_{xy} being finite.

In Fig. 6(a), we have shown the chemical-potential energy-dependent AHC, $\sigma_{xy}(E)$, for FM PrB_4. The obtained $\sigma_{xy}(E)$ is highly nonmonotonic with respect to energy position, and is very large ranging from 500 to 1000 $\Omega^{-1}\,\mathrm{cm}^{-1}$ near E_F ($E = 0$). The peaks and dips in the energy dependence of $\sigma_{xy}(E)$ are expected to arise from the large Berry curvature at the corresponding energy. To explore the origin of such large AHC at E_F, we have examined the Berry curvature $\Omega_{xy}(\boldsymbol{k})$ on the two planes, $k_x = k_y$ and $k_z = 0.098$ Å^{-1}. As plotted in Figs. 6(b) and 6(c), there are multiple sources of Berry curvature. Among them, those near the Γ-Z path in Fig. 6(b) are related to the Weyl points. According to Eq. (2), each Weyl point gives rise to a huge AHC contribution, since

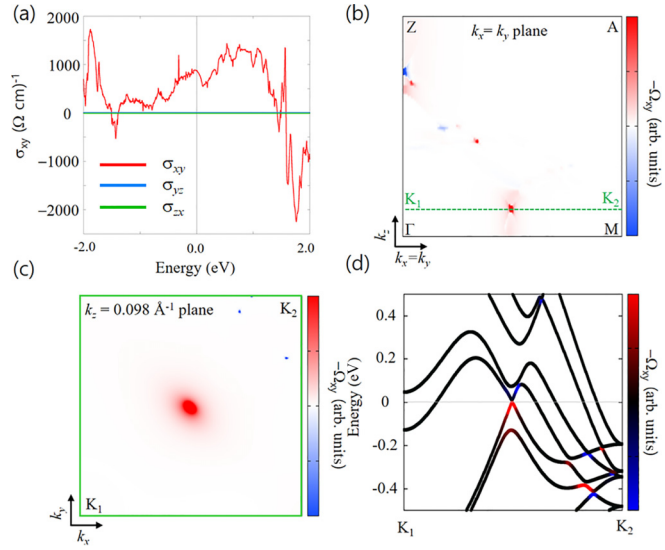

FIG. 6. (a) Chemical-potential energy dependent σ_{xy} for FM PrB_4. (b), (c) Berry curvature $\Omega_{xy}(\boldsymbol{k})$ plot on $k_x = k_y$ and $k_z = 0.098$ Å^{-1} planes at E_F, respectively. K_1 and K_2 are $\boldsymbol{k}$ points on the $k_z = 0.098$ Å^{-1} plane. (d) Band-resolved contribution to $\Omega_{xy}(\boldsymbol{k})$ along the K_1-K_2 path.

$\epsilon_c(\boldsymbol{k}) - \epsilon_v(\boldsymbol{k})$ goes to zero. However, since Weyl points are pair created with opposite chirality, the sum of their Berry curvatures over the whole BZ would vanish.

Noteworthy is that large $\Omega_{xy}(\boldsymbol{k})$ is observed near the center of Γ-M, which becomes the largest near $k_z = 0.098$ Å^{-1} [Fig. 6(c)] would yield a large AHC. Indeed, the band-resolved contribution to $\Omega_{xy}(\boldsymbol{k})$ along K_1-K_2 in Fig. 6(d) clearly indicates that the large Berry curvature and AHC originate from the crossinglike band dispersion located in between K_1-K_2 near E_F. Significantly, a 10 meV gap is present there, implying an anticrossing feature in the band dispersion. Since this contribution does not arise from the Weyl point, and any crystal symmetry $g \in \{P, M_z, C_{4z}\}$ in PrB_4 guarantees $\Omega_{xy}(\boldsymbol{k}) = \Omega_{xy}(g\boldsymbol{k})$, there is no cancellation in the total Berry curvature.

VI. CONCLUDING REMARKS

We predict that a representative FM rare-earth tetraboride, PrB_4, hosts multiple Weyl fermions with various topological charges, namely fourfold-degenerate double-Weyl points with charge ± 2 as well as conventional twofold-degenerate Weyl points with charge ± 1. Such a multitude of topological charges would facilitate PrB_4 to be more advantageous than other MWSs having just conventional single-Weyl nodes, because one can explore stronger topological effects, easier manipulability, and more stability, as in the case of chiral fermion systems with multifold degeneracy. Furthermore, due to its unique temperature-dependent variation of magnetic ordering upon cooling, from PM, AFM, to FM, one can make use of temperature-tuned topological properties of PrB_4. Further experimental studies are encouraged to validate our theoretical predictions and extend our understanding of this fascinating material. Furthermore, our findings hold implications for exploring the topological properties of ErB_4

and TmB_4 since the AFM structures of PrB_4 we investigated in this study are identical to those of ErB_4 and TmB_4 [40].

ACKNOWLEDGMENTS

Helpful discussions with J.-S. Kang are greatly appreciated. D.-C.R. and C.-J.K. were supported by NRF (Grant No. 2022R1C1C1008200) and the KISTI Supercomputing Center (Project No. KSC-2024-CRE-0050). D.-C.R. was supported by NRF (Grant No. RS-2023-00274550). C.-J.K. was also supported by the National Research Foundation of Korea Grant funded by the Korean Government (MOE). K.K. was supported by the internal R&D program at KAERI (No. 524550-24). B.K. acknowledges support by NRF Grants (No. 2021R1C1C1007017 and No. 2022M3H4A1A04074153) and KISTI Supercomputing Center (Project No. KSC-2022-CRE-0465).

[1] X. Wan, A. M. Turner, A. Vishwanath, and S. Y. Savrasov, Phys. Rev. B **83**, 205101 (2011).
[2] B. Yan and C. Felser, Annu. Rev. Condens. Matter Phys. **8**, 337 (2017).
[3] N. P. Armitage, E. J. Mele, and A. Vishwanath, Rev. Mod. Phys. **90**, 015001 (2018).
[4] N. P. Ong and S. Liang, Nat. Rev. Phys. **3**, 394 (2021).
[5] H. Weng, C. Fang, Z. Fang, B. A. Bernevig, and X. Dai, Phys. Rev. X **5**, 011029 (2015).
[6] L. X. Yang, Z. K. Liu, Y. Sun, H. Peng, H. F. Yang, T. Zhang, B. Zhou, Y. Zhang, Y. F. Guo, M. Rahn, D. Prabhakaran, Z. Hussain, S.-K. Mo, C. Felser, B. Yan, and Y. L. Chen, Nat. Phys. **11**, 728 (2015).
[7] A. A. Soluyanov, D. Gresch, A. Wang, Q. Wu, M. Troyer, X. Dai, and B. A. Bernevig, Nature (London) **527**, 495 (2015).
[8] Y. Sun, S.-C. Wu, M. N. Ali, C. Felser, and B. Yan, Phys. Rev. B **92**, 161107(R) (2015).
[9] G. Xu, H. M. Weng, Z. J. Wang, X. Dai, and Z. Fang, Phys. Rev. Lett. **107**, 186806 (2011).
[10] Y. Chen, D. L. Bergman, and A. A. Burkov, Phys. Rev. B **88**, 125110 (2013).
[11] M. Hirschberger, S. Kushwaha, Z. Wang, Q. Gibson, S. Liang, C. A. Belvin, B. A. Bernevig, R. J. Cava, and N. P. Ong, Nat. Mater. **15**, 1161 (2016).
[12] C. Shekhar, N. Kumar, V. Grinenko, S. Singh, R. Sarkar, H. Luetkens, S.-C. Wu, Y. Zhang, A. C. Komarek, E. Kampert, Y. Skourski, J. Wosnitza, W. Scnelle, A. McCollam, U. Zeitler, J. Kübler, B. Yan, H.-H. Klauss, S. S. P. Parkin, and C. Felser, Proc. Natl. Acad. Sci. USA **115**, 9140 (2018).
[13] C. Guo, C. Cao, M. Smidman, F. Wu, Y. Zhang, F. Steglich, F.-C. Zhang, and H. Yuan, npj Quantum Mater. **2**, 39 (2017).
[14] W. Shon, D.-C. Ryu, K. Kim, B. I. Min, B. Kim, B. Kang, B. K. Cho, H.-J. Kim, and J.-S. Rhyee, Mater. Today Phys. **11**, 100168 (2019).
[15] K. Kuroda, M. Ochi, H. S. Suzuki, M. Hirayama, M. Nakayama, R. Noguchi, C. Bareille, S. Akebi, S. Kunisada, T. Muro, M. D. Watson, H. Kitazawa, Y. Haga, T. K. Kim, M. Hoesch, S. Shin, R. Arita, and T. Kondo, Phys. Rev. Lett. **120**, 086402 (2018).
[16] Z. Wang, M. G. Vergniory, S. Kushwaha, M. Hirschberger, E. V. Chulkov, A. Ernst, N. P. Ong, R. J. Cava, and B. A. Bernevig, Phys. Rev. Lett. **117**, 236401 (2016).
[17] I. Belopolski, K. Manna, D. S. Sanchez, G. Chang, B. Ernst, J. Yin, S. S. Zhang, T. Cochran, N. Shumiya, H. Zheng, B. Singh, G. Bian, D. Multer, M. Litskevich, X. Zhou, S.-M. Huang, B. Wang, T.-R. Chang, S.-Y. Xu, A. Bansil, C. Felser, H. Lin, and M. Z. Hasan, Science **365**, 1278 (2019).
[18] K. Kuroda, T. Tomita, M. T. Suzuki, C. Bareille, A. A. Nugroho, P. Goswami, M. Ochi, M. Ikhlas, M. Nakayama, S. Akebi, R. Noguchi, R. Ishii, N. Inami, K. Ono, H. Kumigashira, A. Varykhalov, T. Muro, T. Koretsune, R. Arita, S. Shin, T. Kondo, and S. Nakatsuji, Nat. Mater. **16**, 1090 (2017).
[19] D. F. Liu, A. J. Liang, E. K. Liu, Q. N. Xu, Y. W. Li, C. Chen, D. Pei, W. J. Shi, S. K. Mo, P. Dudin, T. Kim, C. Cacho, G. Li, Y. Sun, L. X. Yang, Z. K. Liu, S. S. P. Parkin, C. Felser, and Y. L. Chen, Science **365**, 1282 (2019).
[20] N. Morali, R. Batabyal, P. K. Nag, E. Liu, Q. Xu, Y. Sun, B. Yan, C. Felser, N. Avraham, and H. Beidenkopf, Science **365**, 1286 (2019).
[21] G. Chang, B. Singh, S.-Y. Xu, G. Bian, S.-M. Huang, C.-H. Hsu, I. Belopolski, N. Alidoust, D. S. Sanchez, H. Zheng, H. Lu, X. Zhang, Y. Bian, T.-R. Chang, H.-T. Jeng, A. Bansil, H. Hsu, S. Jia, T. Neupert, H. Lin, and M. Z. Hasan, Phys. Rev. B **97**, 041104(R) (2018).
[22] D. S. Sanchez, G. Chang, I. Belopolski, H. Lu, J.-X. Yin, N. Alidoust, X. Xu, T. A. Cochran, X. Zhang, Y. Bian, S. S Zhang, Y.-Y. Liu, J. Ma, G. Bian, H. Lin, S.-Y. Xu, S. Jia, and M. Z. Hasan, Nat. Commun. **11**, 3356 (2020).
[23] S. Nie, Y. Sun, F. B. Prinz, Z. Wang, H. Weng, Z. Fang, and X. Dai, Phys. Rev. Lett. **124**, 076403 (2020)
[24] J. Yuan, X. Shi, H. Su, X. Zhang, X. Wang, N. Yu, Z. Zou, W. Zhao, J. Liu, and Y. Guo, Phys. Rev. B **106**, 054411 (2022)
[25] D.-C. Ryu, J. Kim, H. C. Choi, and B. I. Min, J. Am. Chem. Soc. **142**, 19278 (2020).
[26] Y. Hwang, Y. Qian, J. Kang, J. Lee, D.-C. Ryu, H. C. Choi, and B.-J. Yang, npj Comput. Mater. **9**, 65 (2023).
[27] G. A. Wigger, E. Felder, R. Monnier, H. R. Ott, L. Pham, and Z. Fisk, Phys. Rev. B **72**, 014419 (2005).
[28] J. Etourneau, J. P. Mercurio, A. Berrada, and P. Hagenmuller, J. Less-Common Met. **67**, 531 (1979).
[29] G. Kresse and D. Joubert, Phys. Rev. B **59**, 1758 (1999).
[30] G. Kresse and J. Furthmüller, Phys. Rev. B **54**, 11169 (1996); Comput. Mater. Sci. **6**, 15 (1996).
[31] J. P. Perdew, K. Burke, and M. Ernzerhof, Phys. Rev. Lett. **77**, 3865 (1996).
[32] H. C. Choi, A. Laref, J. H. Shim, S. K. Kwon, and B. I. Min, J. Appl. Phys. **105**, 07E107 (2009).
[33] D. Destraz, L. Das, S. S. Tsirkin, Y. Xu, T. Neupert, J. Chang, A. Schilling, A. G. Grushin, J. Kohlbrecher, L. Keller, P. Puphal, E. Pomjakushina, and J. S. White, npj Quantum Mater. **5**, 5 (2020).
[34] See Supplemental Material at http://link.aps.org/supplemental/10.1103/PhysRevB.110.075156 for (i) total energy calculations for different magnetic structures of PrB_4, (ii) calculated spin and orbital magnetic moments of PrB_4 for different J values, (iii)

surface electronic structures of nonmagnetic phase of PrB_4, (iv) band structures of PrB_4 with antiferromagnetic orderings, and (v) effect of a Zeeman-like term in the nonmagnetic open-core calculation.

[35] A. A. Mostofi, J. R. Yates, G. Pizzi, Y. S. Lee, I. Souza, D. Vanderbilt, and N. Marzari, Comput. Phys. Commun. **185**, 2309 (2014).

[36] Q. S. Wu, S. N. Zhang, H.-F. Song, M. Troyer, and A. A. Soluyanov, Comput. Phys. Commun. **224**, 405 (2018).

[37] G. Chang, S.-Y. Xu, B. J. Wieder, D. S. Sanchez, S.-M. Huang, I. Belopolski, T.-R. Chang, S. Zhang, A. Bansil, H. Lin, and M. Z. Hasan, Phys. Rev. Lett. **119**, 206401 (2017).

[38] M. Z. Hasan, G. Chang, I. Belopolski, G. Bian, S.-Y. Xu, and J.-X. Yin, Nat. Rev. Mater. **6**, 784 (2021).

[39] X. Wang, J. R. Yates, I. Souza, and D. Vanderbilt, Phys. Rev. B **74**, 195118 (2006).

[40] L. Ye, T. Suzuki, and J. G. Checkelsky, Phys. Rev. B **95**, 174405 (2017).